Available online at www.sciencedirect.com
SCIENCE DIRECT®
Sensors and Actuators B xxx (2006) xxx–xxx
SENSORS AND ACTUATORS B CHEMICAL
www.elsevier.com/locate/snb

Electroosmosis and thermal effects in magnetohydrodynamic (MHD) micropumps using 3D MHD equations

Vaibhav Patel, Samuel Kinde Kassegne *

Department of Mechanical Engineering, College of Engineering, San Diego State University, 5500 Campanile Drive, San Diego, CA 92182-1323, United States

Received 17 November 2005; received in revised form 28 April 2006; accepted 4 May 2006

Abstract

Magnetohydrodynamics (MHD) micropumps which have no moving parts have attracted attention from the microfluidics community. A significant amount of research is being reported in the design, fabrication and operation of such devices. In this work, we report analytical investigation of the physics of such devices and a development of a generalized numerical framework for the solution of the full 3D MHD equations that govern the multi-physics of MHD micropumps. Based on the numerical framework developed, we investigate different flow channel geometries influenced by the micromachining process, effects of non-uniform magnetic and electric fields, Joule heating, and electroosmosis in MHD micropumps.

Keywords: Microfluidics; Micropumps; Magnetohydrodynamics (MHD); Electroosmosis; Joule heating; BioMEMS; Lorentz force

1. Introduction

Magnetohydrodynamic micropumps as investigated by Lemoff and Lee [1], Jang and Lee [2], Huang et al. [3,4], Heng et al. [5,6], Bao and Harrison [7], Wang et al. [8], Homsy et al. [9], and other researchers have attracted significant attention in the microfluidics community. The basic operating principle of such micropumps is that an electrical current and a perpendicular magnetic field pass through an electrolytic solution; thereby producing a Lorentz force along the length of the channel of the micropump. This force in turn produces a pressure difference in the flow cell that drives the fluid flow. The main reasons for the significant interest in MHD micropumps are the absence of moving parts, simple fabrication processes, lower actuation voltages, reduced risk of clogging and damage to molecular materials, reduced risk of mechanical fatigue and a continuous fluid flow. Subsequently, for quite some time now, there has been a need for comprehensive and rational analytical and numerical procedures that help gain a better understanding of the different fundamental physics of such devices. For macro MHD applications such as marine vehicle propulsion, electromagnetic breaks, nuclear reactor cooling and metal drawing, etc., a wealth of information on rational fluid flow analysis based on the solution of the so-called MHD equations exists [10–12]. In general, these macro-specific MHD equations were solved for a regime of moderate to high Hartmann number (*Ha*, ratio of Lorentz force to viscous forces) and interaction parameters (*N*, ratio of Lorentz force to inertia forces).

However, reports on rigorous analytical and numerical modeling of the MHD equations for microfluidics applications – pertinent to their unique physics and very low Hartmann number regime – are scarce and have just barely begun to appear in the literature. Almost all of these studies had assumed the flow inside such flow cells to be a one-dimensional fully developed laminar flow where Poiseuille type conditions were used to solve for velocity distributions [8]. This assumption of Poiseuille type conditions which neglects the side-wall frictional effects is, however, too simplistic to capture the complex three-dimensional behavior of the fluid flow fields under the most general geometry and magnetic and electric field distribution conditions. As an improvement, Wang et al. [8] used the decoupled and simplified two-dimensional version of the MHD equations where the Lorentz forces were substituted as a pressure in the momentum equations. The ensuing simplified equations were then solved using the finite difference method. Their formulation assumed

* Corresponding author. Tel.: +1 619 594 4046.
E-mail addresses: kassegne@mail.sdsu.edu, samk@digitaladdis.com (S.K. Kassegne).

0925-4005/$ – see front matter © 2006 Elsevier B.V. All rights reserved.
doi:10.1016/j.snb.2006.05.015

an axially invariant velocity distribution; thereby limiting the scope of their numerical solution to channels of uniform cross-section and uniform Lorentz force with no provision for arbitrary channel geometries, and magnetic and electric field distributions. At this point, however, the three-dimensional version of the MHD equations has not been solved yet for MHD micropumps used in microfluidics applications. Furthermore, neither experimental nor theoretical investigations of the effects of electric double layer on the dielectric surfaces of MHD micropumps have been reported in the literature yet. With regard to Joule heating, Homsy et al. [9] have discussed experimental observations where they noted that, beyond a certain current threshold, Joule heating affected velocity measurements; but rational analytical solutions still remain un-attempted.

Therefore, it is clear that the need for defining rational analytical and numerical framework for the solution of the most general 3D MHD equations tailored for the physics and scale of micropumps remains un-met. In this work, we formulate a general numerical framework for the three-dimensional MHD equations for micropumps. With the developed framework, we solve the MHD equations for a variety of geometrical cross-sections of micropumps. The numerical framework makes no simplifying assumptions on the geometry of cross-section and is – therefore – applicable to any potential MHD micropump configuration. Further, we also investigate the effects of double layers (and hence electroosmosis) on the Lorentz force driven fluid flow. We also model Joule heating in the flow cell and investigate the distribution of temperature and effects on the main fluid flow.

To provide a perspective to the range of MHD micropumps considered in this and other studies, Table 1 summarizes some of the typical micropump configurations reported by previous researchers. The table also summarizes the micromachining processes, materials and the geometrical dimensions and reported flow rates. The sizes of the micropumps vary from 2 mm deep [8] to 10 μm × 10 μm [7]. Current and magnetic flux densities vary from a maximum of 140 mA [1] and 2.2 Tesla (T) [6] to 1.8 mA [2] and 420 mT [9]. The flow rates vary from 6010 μl/min for the nozzle/diffuser micropump of Heng et al. [6] to 720 pl/min of Bao and Harrison [7]. Both ac and dc sources have been used. With regard to micromachining processes, bulk micromachining of silicon using LIGA, ICP-RIE (inductively coupled plasma reactive ion etching), and anisotropic wet etching together with soft lithography have been used. Table 1 also demonstrates that MHD micropumps are being increasingly miniaturized with the smallest such device reported currently being at a range of 10 μm. It should be noted, however, that the numerical framework developed in this study is applicable to fluid flow in MHD micropumps where the channel dimensions are 100 μm and higher where Navier–Stokes equations hold true.

2. Three-dimensional physics of MHD micropumps

The physics of magnetohydrodynamics for most macro-level applications is now relatively well developed (Ramos et al., 1986; [10–13]). In the most general form, the physics of electromagnetism and incompressible fluid dynamics are the pre-

Table 1
A summary of some of the recent MHD micropumps reported in the literature

Authors	Micromachining process	Channel material	Geometry of cross-section	Channel dimensions (μm)	Flow rate (Q), I, B, and V
Heng et al. [6]	UV-LIGA and soft lithography	Glass substrate base with PMMA cover plate	Rectangular with diffuser/nozzle	$d = 200,400$; $w_1 = 250$; $w_2 = 500$; $w_3 = 875$; $L = 1000$	ac at 1 Hz, $V = 15$ V; $B = 2.1$ T; $I = 75$ mA; $Q = 1900$, 6010 μl/min
Jang and Lee [2]	Anisotropic bulk-etching of top and bottom wafers—bonded with epoxy	Silicon	Trapezoidal	$d = 400$; $w = 1000$; $L = 40000$	dc field $V = 10$–60 V; $B = 0.44$ T; $I = 1.8$ mA; $Q = 63$ μl/min (measured) = 4 μl/min (predicted) (for 2 mm dia)
Lemoff and Lee [1]	Anisotropic etching	Silicon with glass cover plate	Trapezoidal	$d = 380$; $w = 800$; $L_e = 4000$	ac field at 1 kHz $V = 25$ V; $B = 18.7$ (7.4) mT; $I = 140$, 100 mA; $Q = 18.3$ and 6.1 μl/min (for 1 M NaCl and 0.1 M NaCl)
Bao and Harrison [7]	Bulk micromachining with ICP-RIE	Silicon with O211 glass cover plate	Rectangular	$d = 10$; $w = 10$	ac field at 960 Hz $V = 2$ V; $B = 0.45$ T; $I = 100$ mA; $Q = 720$ pl/min
Wang et al. [8]	No micromachining reported	No micro-machining reported	Rectangular	$d = 2000$; $w = 10000$; $L_e = 35000$	dc at $V = 25$ V; $B = 13$ mT; $I = 140$, 100 mA; $Q = 20.4$ and 14.35 μl/min (for 1 M NaCl and 0.1 M NaCl)
Homsy et al. [9]	Two-step lithography on Pyrex wafers	Pyrex	Semi-circular	$d = 75$; $w = 150$; $L_e = 16000$	dc at $B = 420$ mT; $J = 4000$ A/m^2; $V = 1.27$ mm/s

d: depth of the channel, w: width of the channel (w_1 and w_2 for trapezoidal channels are widths at top and bottom), L: length of the channel, L_e: the length of the electrode, B: magnetic flux density, I: current, Q: flow rate; V: electric potential.

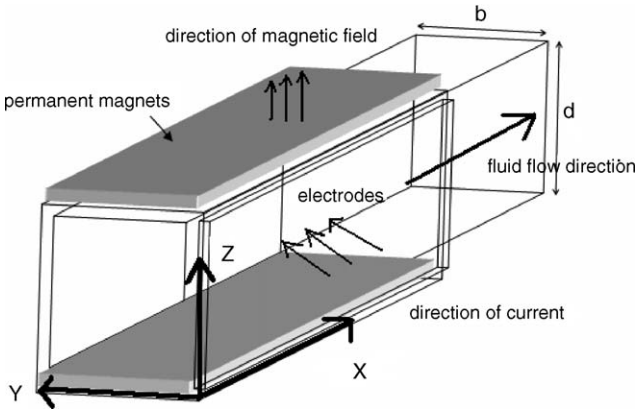

Fig. 1. Typical configuration of MHD micropump with a rectangular cross-section.

dominant physics of interest for macro-level MHD applications. For MHD micropumps which are typically of several hundred of microns dimensions and fabricated using MEMS processes such as silicon/glass bulk micromachining and soft lithography (Fig. 1 and Table 1), however, their unique scale and material properties require that additional physics be accounted for to accurately capture their behavioral response to external effects. One such physics is electroosmosis which is the bulk movement of an aqueous solution under an external electric field [14]. In MHD micropumps – much like most microfluidic devices – electroosmosis is caused by the existence of a zeta potential at the interface between the silicon or glass linings and the electrolyte. This zeta potential is formed due to the dissociation of ions or ionic groups and extends over a thin layer at the interface between the glass/silicon/metal linings of the micropump and the electrolyte. This thin layer is called an electrical double layer and has a typical thickness of less than 10 nm (Debye's length). Another physics that is considered in this study is the physics of Joule heating. Typically, in a conductive media such as an electrolyte, an electric field causes heating and change in temperature distribution. This change in temperature will in turn cause a decrease in viscosity and increase in conductivity of the electrolyte. A 2% increase in conductivity per degree rise in electrolyte temperature is considered a typical value [25]. For the dependency of viscosity on temperature in electrolytes such as low concentration saline solutions (1 M NaCl), the models used for water could be adopted [15]. Further, thermal heating of an electrolyte also causes electrothermal forces that contribute to fluid velocity increases [16].

For deriving a more-general MHD set of equations applicable for MHD micropumps and a numerical framework for their solution, the general MHD equations such as those reported by Hughes et al. [10] serve as a starting point. Four distinct sets of equation systems are considered here; electromagnetic system, fluid dynamic system, electrokinetic system and a thermal system. The electromagnetic system consists of the Gauss law and magnetic induction equation along with Poisson's equation and Ohm's law. These equations (i.e., Eqs. (1.a)–(1.e)) define the distribution of the magnetic flux density, the electric field and the current density, respectively. In its general form, the magnetic induction equation suggests that the motion of a conducting liquid (electrolyte) in an applied magnetic field induces a magnetic field in the medium through a $\nabla \times (\mathbf{U} \times \mathbf{B})$ term, where $\mathbf{U}$ is the velocity field and $\mathbf{B}$ is the magnetic flux density. The total magnetic field is, therefore, the sum of the applied and induced magnetic fields. The relative strength of the induced field is often characterized by a dimensionless number; the magnetic Reynolds number, $Re_m, = \sigma \mu_m UL$ where σ is the electrical conductivity, μ_m the magnetic permeability, U the velocity and L is the length of the channel. For typical electrolytes used in biological microfluidics applications, Re_m is small and, therefore, the induced magnetic field is often neglected as is the case in this work.

The fluid dynamic system consists of the continuity equation and Navier–Stokes equation that define the physics of bulk fluid flow (Eqs. (3.a) and (3.b)). Helmholtz–Smoluchowski equation for electroosmotic flows (Eq. (4)) forms the electrokinetic system whereas the energy balance equation (Eq. (5.a)) and the time averaged electrothermal force equation, given by Eq. (5.b) [16], form the thermal system. In Eq. (5.b), the first part is the Coulombic force dominant at low frequencies whereas the second part is the dielectric force dominant at higher frequencies (and also dc). Combined together, the full three-dimensional MHD equations that govern the physics of MHD micropumps including the reverse Lorentz force, the non-zero zeta-potential on flow channel walls and Joule heating are given by Eqs. (1)–(5). These equations are coupled. The boundary conditions for each of the equation systems are given in Table 2.

To solve these equations in an iterative manner, the following assumptions are made. The flow is assumed to be fully developed and laminar (low Reynold's number) with no recirculating flow. The fluid has low conductivity; as the fluids of interest are typical electrolytes used in biological applications. Consequently, the Hartmann number, Ha $(\sigma B^2 L^2/\mu)^{0.5}$ and the interaction parameter, N $(\sigma B^2 L/\rho U)$ are both small (where σ is the electric conductivity of fluid, μ the viscosity, ρ the density of fluid, L the length of channel, and B and U are the magnetic flux density and velocity field, respectively, as defined earlier). The current induction from a moving fluid under a magnetic field is assumed to be negligible; thereby decoupling the magnetic induction and magnetic line closure relationships [10,17]. Further, the Debye length (often in the range of 10 nm or so) is assumed to be very small compared to the channel width. This enables the use of the Helmholtz–Smoluchowski equation to represent electroosmosis. Under these assumptions, then, the full 3D MHD equations for an isotropic incompressible Newtonian fluid used in a micro-scale are formally written as follows:

(i) Electromagnetic system

The magnetic field components are given as

$$\nabla \cdot B = 0 \quad \text{(Gauss law/magnetic line closure)} \tag{1.a}$$

$$\frac{\partial B}{\partial t} = \frac{1}{\sigma \mu} \nabla^2 B \quad \text{(magnetic induction)} \tag{1.b}$$

Table 2
Boundary conditions for generalized 3D rectangular MHD equations for MHD microfluidics pumps

Electromagnetics
$B(x,y,0)$ = known (+) ($x < L_e$)
$B(x,y,d)$ = known (−) ($x < L_e$)
Electrodes
$\Phi(x,0,z) = V$ ($x < L_e$)
$\Phi(x,b,z) = -V$ ($x < L_e$)
Insulations
Magnetically insulated elsewhere
Electrically insulated elsewhere
Fluid dynamics
$U(x,0,z) = 0$ (no-slip), $U(x,y,0) = 0$ (no-slip)
$U(x,b,z) = 0$ (no-slip), $U(x,y,d) = 0$ (no-slip)
Inlet
$U(0,y,z) = 0$
Outlet
$P(L,y,z) = 0$
Body force = $\mathbf{F}_L$ (Lorentz force)
Electrokinetics
$U(x,y,0) = U_{EO}$ (slip)
$U(x,y,d) = U_{EO}$(slip)
Thermal system
$T(x,y,0)$ = room temperature 25 °C (isothermal with outside) at bottom magnet
$T(x,0,z)$ = room temperature 25 °C (isothermal with outside) at electrode
$T(x,b,z)$ = room temperature 25 °C (isothermal with outside) at electrode
$T(x,y,d) = k\Delta T$ (free convective flux) at top magnet
$Q(0,y,z)$ = zero flux where Q is the heat flux
$Q(1,y,z)$ = zero flux

The electrical field components are

$$\nabla^2 \Phi = \nabla \cdot (\mathbf{U} \times \mathbf{B}) \quad \text{(Poisson's equation)} \tag{1.c}$$

$$E = -\nabla \Phi \tag{1.d}$$

$$J = \sigma(E + \mathbf{U} \times \mathbf{B}) \quad \text{(Ohm's law)} \tag{1.e}$$

The Lorentz force is then given as

$$\mathbf{F}_L = (J \times B) L_e \tag{2}$$

(ii) Fluid dynamics system

$$\nabla \cdot U = 0 \quad \text{(continuity equation)} \tag{3.a}$$

$$p\left(\frac{DU}{Dt} + U \cdot \nabla U\right) = -\nabla p + \mu \nabla^2 U + \mathbf{F}_L + \mathbf{F}_{ET}$$

(Navier–Stokes equation) (3.b)

(iii) Electrokinetic system

$$U_{EO} = -\mu_{EO} \nabla \Phi, \quad \text{where } \mu_{EO} = \frac{\varepsilon \zeta}{\mu}$$

(Hemholtz–Smoluchowski equation) (4)

(iv) Thermal system

$$\rho C_p \left(\frac{DT}{Dt} + U \cdot \nabla T\right) = k \nabla^2 T + \frac{J^2}{\sigma} \tag{5.a}$$

$$F_{ET} = -\frac{1}{2}\left[\left\{\frac{\nabla\sigma}{\sigma} - \frac{\nabla\varepsilon}{\varepsilon}\right\} E \frac{\varepsilon E}{1 + (\omega\tau)^2} + \frac{1}{2}|E|^2 \nabla\varepsilon\right] \tag{5.b}$$

where p is the fluid pressure, J the current vector, T the temperature, t the time, Φ the electric potential, E the electric field, U_{EO} the electroosmotic velocity, μ_{EO} the electroosmotic mobility, Cp the specific heat, k the thermal conductivity, ζ the zeta potential, ε the dielectric permittivity, $\tau = \varepsilon\sigma$ the charge relaxation time of fluid, ω the frequency of the ac electric field, L_e the electrode length, $\mathbf{F}_{ET}$ the electrothermal force, and $\mathbf{F}_L$ is the Lorentz force.

For steady-state conditions, the left hand sides of Eqs (3.b) and (5.a) reduce to zero. The 3D MHD equations given here are conveniently solved using any finite element discretization approach. FEMLAB FEMLAB (COMSOL, 2005) multiphysics FEA modeling software is used for the solution of these equations. The mesh sizes differ depending on the geometry under consideration; however quadratic elements are used with enough refinement for convergence. Due to the coupling between these sets of equations, an iterative solution approach is used. First, the electromagnetic components as given by the Gauss law and the magnetic induction law (Eqs. (1.a) and (1.b)) are solved to determine the magnetic flux density (**B**). It is instructive to recognize that these equations form part of the Maxwell equations [17]. The electric potential (Φ), the electric field (**E**) and current densities (**J**) are then determined by solving the Poisson equation and Ohm's law (Eqs. (1.c)–(1.e)). In the initial run, the component of the current density that comes from the cross product of the velocity and the magnetic field (i.e., $\mathbf{U} \times \mathbf{B}$) is zero as the fluid velocity is not yet determined. The Lorentz force is then evaluated as a vector cross product of the current vector and the magnetic flux density vector (Eq. (2)). The Lorentz force is then applied as a body force in the Navier–Stokes equation. This is followed by the solution of the three-dimensional continuity and Navier–Stokes equations (Eqs. (3.a) and (3.b)). Once the vectorial flow velocity distribution (**U**) is determined, the electrical field components (i.e., Φ, **E** and **J**) are re-evaluated by adding the current component from the vector cross product of the velocity and the magnetic field (i.e., $\mathbf{U} \times \mathbf{B}$) to Eqs. (1.c)–(1.e). Subsequently, for a given iteration, the thermal system is solved using Eq. (5.a); the quantity of interest being the temperature profile (T). The Lorentz's force $\mathbf{F}_L$ and the electrothermal force $\mathbf{F}_{ET}$ (Eq. (5.b)) are then updated and the Navier–Stokes equations are re-solved. This iterative process is repeated until the velocity (**U**), the temperature (T), and the electric field (**E**) converge to within a pre-set cutoff limit. Here a cut-off limit of $|U_{n+1} - U_n|/|U_n| \leq 1.0 \times 10^{-6}$, $|E_n + 1 - E_n|/|E_n| \leq 1.0 \times 10^{-6}$, and $|T_n + 1 - T_n|/|T_n| \leq 1.0 \times 10^{-6}$ are used where n and $n + 1$ represent the iteration numbers. The electroosmotic velocity component ($\boldsymbol{U}_{EO}$) is determined using the Helmholtz–Smoluchowski equation given in Eq. (4).

3. Numerical results and discussions

To validate and establish the accuracy of the proposed numerical framework for the solution of the generalized 3D MHD equations for micropumps, a number of numerical examples are

solved. A low conductivity electrolyte (1 M NaCl solution) is considered in these examples.

The first problem solved here to establish the accuracy of the equations is an example taken from Homsy et al. [9] where the length of the channel is 20 mm, with length of electrode of 16 mm, channel width of 150 μm and the depth of 75 μm. The current density ($\mathbf{J}$) = 4000 A/m^2. The magnetic flux density ($\mathbf{B}$) = 0.42 T. For this problem and all other numerical solutions reported here, the following properties are used for a low conductivity fluid (1 M NaCl): permittivity (ε) = 6.95e−10 C^2/Jm, density (ρ) = 1030 kg/m^3, dynamic viscosity (η) = 6e-4 N s/m^2, fluid conductivity (σ) = 1.5 S/m, thermal conductivity (k) = 0.6 W/m/K and specific heat capacity (Cp) = 2300 J/(kg K).

A maximum velocity of 1.08 mm/s is determined by the full 3D MHD equations whereas Homsy et al. [9] report a maximum calculated velocity of 1.2 mm/s (average velocity of 0.6 mm/s) and experimentally observed velocity of 1 mm/s. This demonstrates the application and validity of the MHD equations developed in this study.

3.1. Rectangular channel MHD micropump

The simplest geometry for MHD micropumps is a rectangular cross-section and is, therefore, used here to validate the solutions for the MHD framework proposed in this work. As indicated in Table 1, such geometry of flow cell has been used in the works reported by Wang et al. [8], Heng et al. [6] and Bao and Harrison [7]. Micromachining processes that enable a rectangular flow cell in MHD micropumps are typically UV-LIGA or DRIE (deep reactive ion etching) of silicon or glass substrates. The permanent magnets are placed at the top and bottom of the channel with electrodes placed on the sides of the channels. Due to the non-variance of the velocity field in the axial direction, the problem actually reduces to a two-dimensional flow problem. The ensuing magnetic and electric fields are uniform resulting in a Lorentz force that is in-turn uniform across the channel cross-section.

In the example problem considered here, the length of the channel is 45 mm, with an electrode length of 35 mm. The width is 1000 μm and the depth is 500 μm. A constant current mode of operations is considered with current ($\mathbf{I}$) of 0.01 A. The magnetic flux density ($\mathbf{B}$) = 18 mT. The zeta potential ($\boldsymbol{\zeta}$) is assumed to be 100 mV.

The maximum velocity in the channel is determined to be 3.45 mm/s with the velocity assuming the typical parabolic distribution of pressure-driven flows. The Hartmann number, Ha, has a low value of 0.001 ($1.5 \times 0.018^2 \times 0.0352/6e{-}4$) for this biological fluid primarily because of the very low electrical conductivity, σ. The reverse Lorentz's force $(\sigma(U \times B) \times B)L_e$ given by Eqs. (1.e) and (2) is therefore negligibly small and does not produce the M-shaped velocity profile that is expected in fluid flows of high Hartmann number [10]. A parametric study on the variation of the velocity with the depth of the channel for a series of fixed width values is given in Fig. 2. With current and magnetic flux density kept constant at 0.01 A and 18 mT, respectively, the velocities, in general, increase with increasing

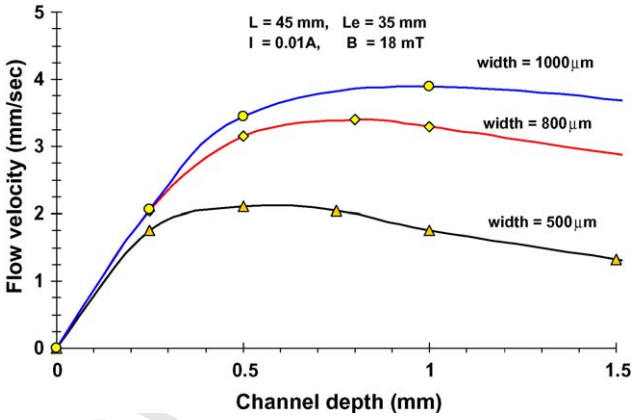

Fig. 2. Dependence of flow velocity on depth in rectangular channels of different widths. The current is 0.1 A and the magnetic flux density is 18 mT.

depth until peak values are reached when the depths are equal to the respective widths. Following the peak values, the velocities are observed to decrease due to the reduction in current densities. These families of curves could serve as design guides as they demonstrate the effect of geometry in optimizing the flow velocity in MHD pumps.

The effect of electroosmosis on the fluid flow pattern and magnitude is next investigated. In MHD micropumps, it is the top and bottom glass or silicon linings that typically possess a non-zero zeta potential that drives an electroosmotic bulk fluid flow. For example, in some of the MHD micro pumps reported in the literature [1], the top of the channels are made of glass that is bonded to silicon. The glass surface typically has a non-zero zeta potential. The transverse electroosmotic flow occurs in the volume between the side electrodes along the direction of the electric field with its velocity determined by the magnitude of the electric field as given by the Helmholtz–Smuluchowski equation. It is important to note that the electroosmotic flow is in the transverse direction as opposed to the longitudinal fluid flow due to Lorentz's force. For this electroosmotic study, we have used MHD pump of rectangular cross-section geometry with width of 100 μm, depth of 100 μm, centrally located electrode length of 5 mm, and total pump length of 11 mm as shown in Fig. 3 [19]. The current used is 0.01 A with magnetic flux density of 18 mT and zeta potential of 0.1 V. The electroosmotic velocity (V_{EO}) is evaluated by the Helmholtz–Smoluchowski equation (Eq. (4)) to be 1.57 mm/s (note that we now use the designation V_{EO} to denote that the electroosmotic velocity is in

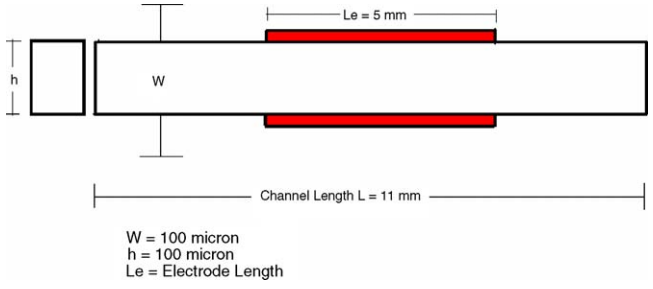

Fig. 3. Dimensions of MHD channel considered for evaluation of electroosmotic velocities [19].

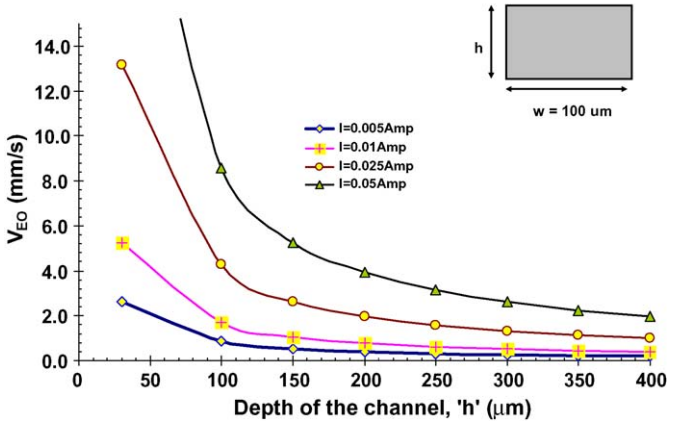

Fig. 4. The effect of depth reduction on the electroosmotic velocity (V_{EO}) in rectangular MHD micropump.

the global *y*-direction as given in Fig. 1). On the other hand, the main Lorentz's flow in this geometry of MHD pump was found to be about a mere 15 μm/s. The effect of scaling of the depth on electroosmotic velocity is studied by varying the depth from 400 μm down to 30 μm. Fig. 4 shows that the electroosmotic velocity increases quadratically with the decrease in the depth of the channel. For current levels of only 0.025 A, electroosmotic velocity of as much as 2 mm/s is predicted for channel depth of 200 um. For smaller depths such as 30 μm, the electroosmotic velocity increases to as much as 5.5 mm/s for a current of 0.01 A and 13.2 mm/s for a current of 0.025 A. The magnitude of electroosmotic velocities could, therefore, be very significant in MHD micropumps, particularly for shallow depths.

3.2. Nozzle/diffuser channel MHD micropump

For ac-type magnetohydrodynamic micropumps, it has been reported that the integration of a diffuser/nozzle component with the MHD driving chamber significantly reduces the backflow thereby increasing the net flow of the fluid that is being pumped (Heng et al., 2001; Murphy and Lian, 2001; [5,8]). Microvalves based on diffuser/nozzle components have been reported by previous researchers as well (Gerlarch, 1998; [20,21]). Heng et al. (2001) had investigated the arrangement of such pumps in series and parallel and different length of the pumping sections as well as different channel heights and widths for maximum flow rate.

We implement the three-dimensional numerical framework outlined in this work to determine flow velocities and flow rates in such pumps with a typical geometry given in Fig. 5. The effect of the diffuser/nozzle configuration on the distribution of magnetic and electric fields and hence the Lorentz force is investigated. The length of Pump, L ($=a+a+b+a$) is 16 mm with the electrode length of 4 mm in the throat section, diffuser length of 8 mm and exit length of 4 mm. The width of the pump is 800 μm and the depth is 800 μm. A current (**I**) of 0.1 A and magnetic flux density (**B**) of 18 mT are applied.

The maximum calculated velocity is 15.2 mm/s. The variation of the velocity along the direction of the channel is given in Fig. 6 that indicates a slight velocity increase due to entrance effect in

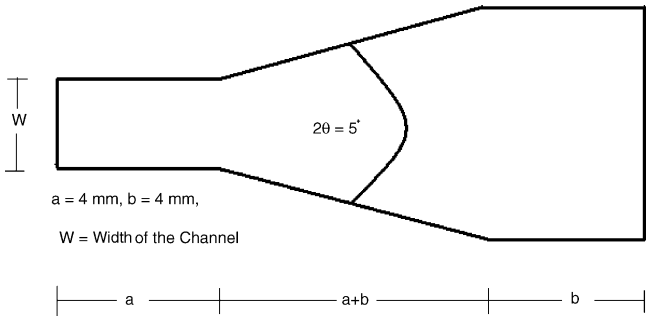

Fig. 5. Geometry of nozzle/diffuser section.

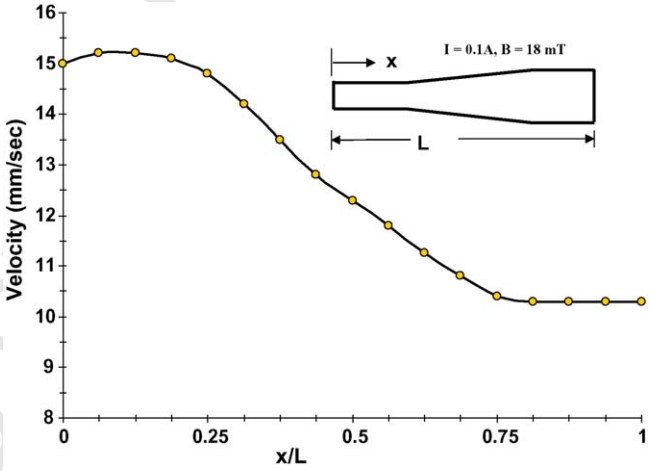

Fig. 6. Velocity distribution along the channel length of a nozzle/diffuser flow cell. The velocity increases within the first 4 mm length (throat where the electrodes are located) and then decreases in the diffuser section.

the pump section (where the electrodes are placed) followed by a decrease in the diffuser section and a flat velocity in the channel section. A parametric study on the variation of the velocity with the depth of the channel for a series of width values are given in Fig. 7. In general, the figure demonstrates that the effect of depth and width on the flow velocities in nozzle/diffuser channels is similar to rectangular channels.

The contribution of the ($\mathbf{U} \times \mathbf{B}$) term towards the current density (**J**) is then investigated to validate our earlier assump-

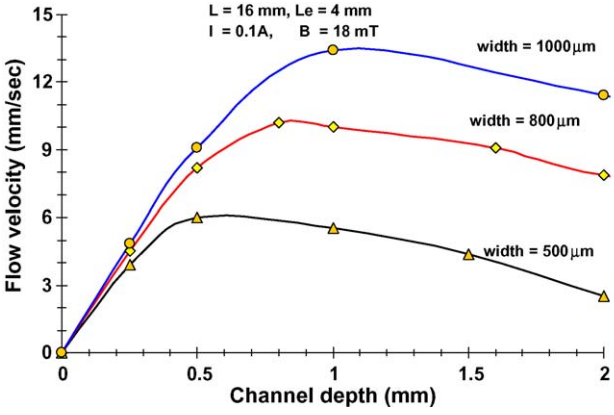

Fig. 7. Dependence of velocity on depth in nozzle/diffuser shaped channels of different widths.

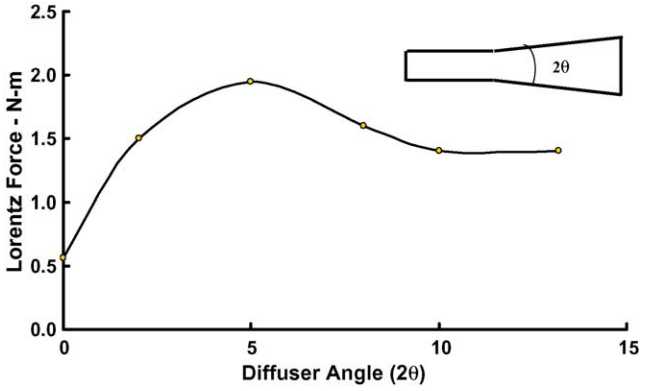

Fig. 8. Dependence of velocity on diffuser angle in nozzle/diffuser shaped channels.

tion which neglected this quantity. The solution of the 3D MHD equations yielded a magnitude of ($\mathbf{U} \times \mathbf{B}$) term (i.e., 15.2e−3 m/s × 18e−3 T) which is in the order of 2.5×10^{-4} to 4.0×10^{-4} V/m and is considered negligible. With regard to current density ($\mathbf{J}$), only the first 4 mm section of the pump which has electrodes experiences significant current density values whereas the diffuser section has negligible amount. The effect of the diffuser angle on the magnitude of the velocities is also investigated and a summary of the results presented in Fig. 8. For a given depth, a maximum velocity is obtained when the diffuser angle (2θ) is about 5°. This angle corresponds to a minimum frictional loss in the channel. A similar value of 5° has been reported by other researchers in valveless diffuser pumps [20,22].

3.3. Trapezoidal channel MHD micropump

In typical silicon as well as glass micromachined channels, the MHD pump is fabricated through a wet anisotropic etching of a V-groove through a silicon wafer [1,2]. This results in a typical trapezoidal cross section of the flow channel with the side channels assuming a typical angle of $\alpha = 54.7°$. The electrodes which are typically deposited on the side walls are – therefore – non-parallel while the magnets are typically placed on the top and bottom of the flow cell in a parallel fashion.

In a trapezoidal cross-section MHD pump example considered here, the length of the channel is 4 mm, which is the same as length of electrode. The top width is 800 μm with a bottom width of 340 μm and a depth of electrode of 400 μm. Note that the actual depth of the channel is then 326 μm. A constant voltage mode is assumed here where instead of the current, the voltage is held constant. A potential of 1.5 V is applied at the anode whereas −1.5 V is applied at the cathode. This corresponds to an average current of 0.01 A. The magnitude of the magnetic flux density is 18 mT. The current density distribution is given in Fig. 9 whereas the magnetic flux density is given in Fig. 10. The two figures indicate that both the current density and the magnetic flux density are not uniform at any given cross-section of the micropump with their maximas typically occurring at the corners. The Lorentz force is non-uniform and in fact assumes a 'M' shape distribution at the flow cell cross-sections as shown in Fig. 11.

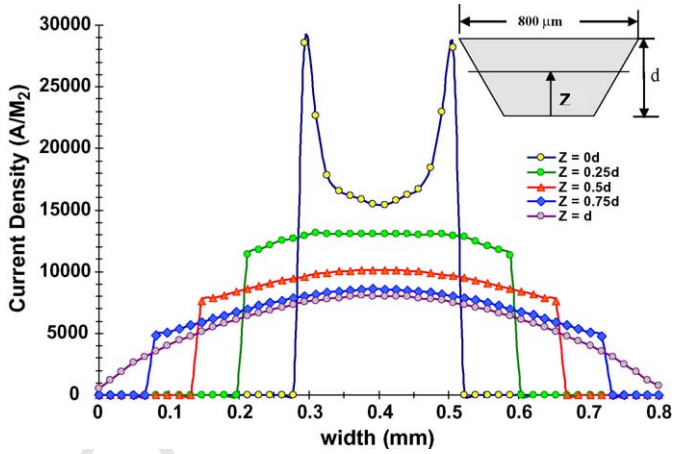

Fig. 9. Current density (J/Area) distribution in a cross-section of a trapezoidal channel at different depths. d is the depth of the channel. Due to the prismatic geometry of the flow-cell, the same distribution will occur at any cross-section along the length.

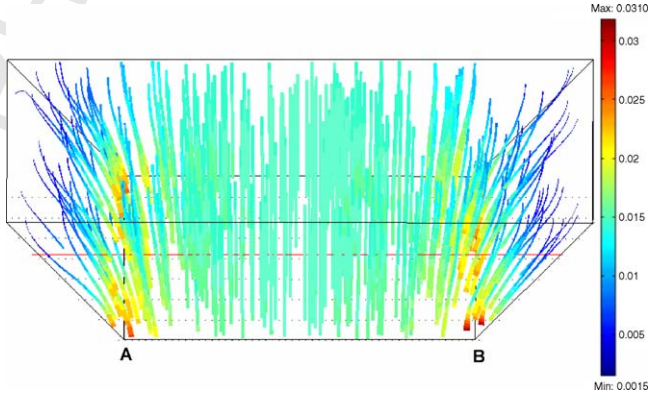

Fig. 10. Streamlines of magnetic flux density in a trapezoidal shaped MHD pump. In the middle region of the flow-cell, the magnetic flux density assumes uniform magnitude and direction. However, due to the sloping sides, the magnetic flux is distorted towards the sharp corners at the bottom of the flow-cell. The magnetic flux density is also highest at the edges, A and B. The flux density is given in Tesla.

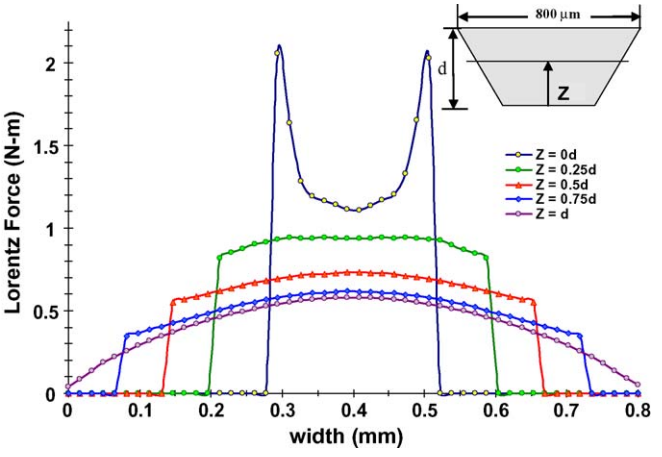

Fig. 11. Lorentz force ($\mathbf{F}_L$) distribution in a cross-section of a trapezoidal channel at different depths. Due to the prismatic geometry of the flow-cell, the same distribution will occur at any cross-section along the length.

Table 3
Comparison of flow rate, maximum velocity and Lorentz's force in MHD micropumps of trapezoidal and rectangular cross-sections at mid-span of channel

Cross-section	Maximum velocity (m/s)	Current (A)	Magnetic flux density (T m^2)	Lorentz's force (N m/m)	Flow rate, Q (μl/min)
Trapezoidal: top width = 800 μm; bottom width = 340 μm; depth = 326 μm	1.86e−3	0.00147	1.86e−9	1.60e−5	9.06
Rectangular: width = 570 μm; depth = 326 μm	1.69e−3	0.00147	2.10e−9	1.66e−5	9.25
Trapezoidal: top width = 1000 μm; bottom width = 575 μm; depth = 350 μm	1.65e−3	0.00157	2.53e−9	1.61e−5	11.73
Rectangular: width = 787.5 μm; depth = 350 μm	1.54e−3	0.00157	2.84e−9	1.69e−5	12.25

Channel length as well as electrode lengths are 4 mm. Note that the magnetic flux density is integrated over a cross-section and hence the unit is T m^2.

The flow velocities in trapezoidal cross-section MHD micropumps are then compared with those of rectangular cross-section pumps. The intent is to investigate the change in flow velocities while keeping the area of cross-sections and volume as well as electrode and channel lengths constant. In the first example, the same dimensions of the trapezoidal channel (800 μm top width, 340 μm bottom width and 326 μm depth) are considered while the rectangular cross-section micropump has an equivalent area of cross-section with 326 μm depth and 570 μm width. The electrode lengths and total channel lengths in both cases are 4 mm. The potentials at the anode and cathode in both geometries are 1.5 and −1.5 V, respectively. In both geometries of channels, the magnetic flux density is generated through application of magnetic potentials of 1.5 A (Amperes) and −1.5 A at top and bottom magnets.

The solution of the full 3D MHD equations for both trapezoidal and rectangular cross-section MHD micropumps is then carried out under these equivalent conditions for all the physics under consideration. Table 3 summarizes the results in maximum velocity, flow rate, Lorentz's force, magnetic flux density and current at a cross-section taken at half-length of the micropumps. Our results indicate that the flow rate in trapezoidal cross-section micropumps is comparable to that of rectangular cross-section pumps unlike the results reported by like Bao and Harrison [7] who used an approximate formula for macro channels to report differences as high as a factor of 3. The results from this analysis which is based on rigorous accounting of all the multi-physics in MHD micropumps, therefore, demonstrate – for the first time – that trapezoidal cross-section micropumps offer as good flow rate as rectangular cross-sections. Table 3 also shows that the maximum velocity evaluated in trapezoidal micropumps is slightly higher than those in rectangular micropumps. In the dimensions considered here, the variations were between 7 and 10%. On the other hand, the flow rates in rectangular micropumps are evaluated to be slightly higher than those of trapezoidal cross-section micropumps. The variations are, however, less than 5% for the dimensions considered suggesting that trapezoidal cross-section MHD micropumps which are easy to micromachine [1] are as efficient as rectangular MHD micropumps. Further, Table 3 summarizes that the total net current and magnetic flux densities at a given cross-section of these micropumps are comparable with their differences being less than 10% in the case of magnetic flux density and nil in the case of total current. The Lorentz's force – which is a direct function of the magnetic flux density and current density – is, therefore, of comparable magnitude in both rectangular and trapezoidal cross-section micropumps.

The effect of electroosmosis on the fluid flow pattern and magnitude is investigated next. For this electroosmotic study, we have used MHD pump of trapezoidal cross-section geometry with width of 800 μm, depth of 380 μm, electrode length of 4 mm, and total channel length of 20 mm. The current used is 0.01 A with magnetic flux density of 18 mT and zeta potential of 0.1 V. The main Lorentz's flow in this geometry of MHD pump was found to be about 0.5 mm/s. The electroosmotic velocity (V_{EO}), on the other hand, is evaluated by the Helmholtz–Smoluchowski equation (Eq. (4)) to be 0.6 mm/s—the same order as the main flow for this particular current density. The effect of scaling of the depth on electroosmotic velocity is studied by varying the depth from 400 μm down to 30 μm. Fig. 12 shows that the electroosmotic velocity increases quadratically with the decrease in the depth of the channel as is the case for rectangular MHD pumps. For current levels of only 0.025 A, electroosmotic velocity of as much as 3.0 mm/s is predicted for channel depth of 200 μm. For smaller depths such as 30 μm, the electroosmotic velocity increases to as much as 7.6 mm/s for a current of 0.01 A.

3.4. Effect of Joule heating

One of the main physics considered in this study is that of Joule heating with the objective of determining its influence on the fluid flow. For illustrative purposes, we consider a rectangular

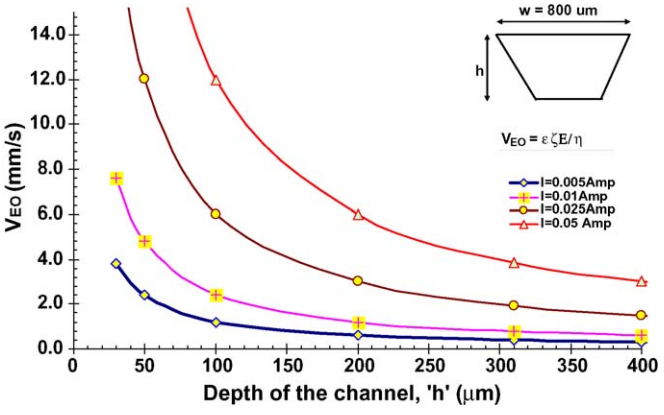

Fig. 12. The effect of depth reduction on the electroosmotic velocity (V_{EO}) in a trapezoidal MHD micropump.

cross-section MHD pump. For simplicity, our model considers heat transfer only in the micropump region neglecting the effect of thermal diffusion to a significant part of the whole chip which contains the MHD micropump. As a result, our model will give temperature distributions which are an upper bound solution; but nevertheless offer a good insight to the effect of Joule heating. The thermal boundary conditions are given in Table 2. The bottom magnet and the two side electrodes shown in Fig. 1 are assumed to be fixed at room temperature since, in most experiments, the chip sits on a relatively large flat surface area [15]. The top magnet is exposed to the outside environment and a free convection boundary condition is assumed. Zero flux conditions are assumed at the entrance and exit of the micropump channel.

The dependency of viscosity and conductivity on temperature are accounted for using Eqs. (6) and (7):

$$\ln\left(\frac{\eta}{\eta_0}\right) = -1.704 - 5.306\left(\frac{273}{T}\right) + 7.003\left(\frac{273}{T}\right)^2 \quad (6)$$

$$\sigma_T = \sigma(1 + 0.02T) \quad (7)$$

where η is the viscosity in N s/m^2, η_0 the viscosity at room temperature and T is the temperature in Kelvin. Note that Eq. (6) which is applicable for water is extended for use for the biological electrolyte considered in this study by using a proportionality factor of 0.6 to account for the ratio of viscosity of water to 1 M saline solution at room temperature. Fig. 13 shows the range of temperature changes predicted in a rectangular MHD micro-pump discussed in Section 3.1. The figure shows that temperature increases as much as 20 °C and more are possible in rectangular cross-section MHD pumps for channels of depths of 30 μm and width of 100 μm when subjected to a current of 0.025 A. The Joule heating is, of course, a function of J^2/σ (Eq. (5.a)); therefore significant temperature rises are predicted for micropumps with increased current densities as in shallow channels. Given the fact that the conductivity of most biological electrolytes increases by 2% for each degree rise in temperature [25], the 20 °C rise in temperature in shallow rectangular channels reported here can effectively increase the fluid conductivity locally by as much as 40%. This will in turn lead to

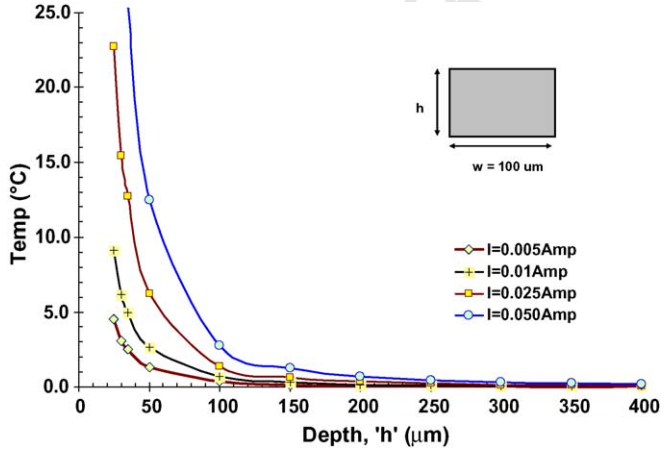

Fig. 13. The effect of depth reduction on Joule heating in rectangular MHD micropump. T is the temperature rise in °C.

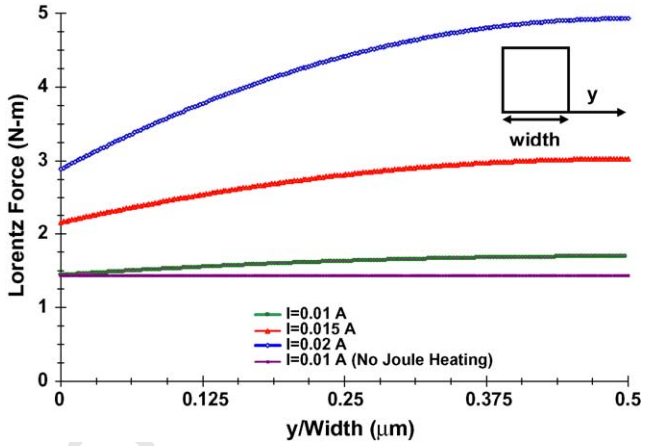

Fig. 14. The effect of Joule heating on the Lorentz's force in rectangular MHD micropump. The Lorentz force is calculated at the center of the pump.

increases in current strength and hence Lorentz's force and fluid flow velocity in MHD micropumps. The fluid velocity is also further increased by a decrease in viscosity. Analysis was carried where the full 3D MHD equations developed in this study were solved considering the conductivity and viscosity changes with temperature (i.e., Eqs. (6) and (7)). Due to the increased conductivity, the current density and hence the Lorentz force across the cross-section of the micropump increase as shown in Fig. 14. It is instructive to note that the resulting Lorentz force has a parabolic distribution across the width of the channel. This is not surprising since the ensuing temperature profile (and therefore the conductivity, σ_T) in the presence of Joule heating assumes such distribution. This parabolic distribution of the temperature profile has been discussed in detail by Petersen et al. [25]. Fig. 14 shows that for current levels of 0.01, 0.015, and 0.025 A, the average increases in the Lorentz force in the pump section are 20%, 30% and 44%, respectively. Further, decreases in viscosity of as much as 20% for channel depths of 50 μm and width of 100 μm under a current of 0.025 A were observed due to Joule heating which in turn contribute to a proportional increase in flow velocity. The results from this study, therefore, suggest that the effects from Joule heating could be significant enough to warrant consideration, particularly for shallow MHD micropumps where the current densities are high.

4. Conclusions

In this study, we have developed a complete numerical framework for the three-dimensional MHD equations that govern the behavior of MHD micropumps. This is expected not only to fill the gap that has existed for sometime now in the area of prediction and optimization of the behavior of such micropumps under differing geometric configurations, electric fields and magnetic flux densities but also provide a useful analytical tool to investigate newer configurations and designs. Our research indicates that:

(a) Transverse electroosmotic flows could have a considerable effect on the efficiency of axial MHD pumps especially for MHD micro-pumps with shallow channels and high current

density. In some cases, the electroosmotic velocity could be significantly higher than the main Lorentz flow. Electroosmotic flow in a high current density dc MHD pump was experimentally observed and reported by Homsy et al. [9]. This current study is, however, the first work that uses rational analytical expressions to predict this flow.

(b) Joule heating has a significant effect on the flow velocity of MHD micropumps, especially for pumps with shallow depths and higher current density. As much as 20 °C increase in the temperature of the electrolyte are predicted for high current densities. Again, Joule heating has been experimentally observed by Homsy et al. [9]. Our work is the first to quantify this heating.

(c) Joule heating is observed to in-turn increase the conductivity but decrease the viscosity of the electrolyte. The increase in electrolyte conductivity in turn translates to increased current densities and hence Lorentz forces and flow velocity. The decrease in the electrolyte viscosity also leads to increased flow velocity.

(d) In almost all the research reported in MHD micro-pumps, the magnetic and electric fields are assumed to be uniform. However, due to the non-alignment of the magnets with the electrodes and defects in the geometry of the channels during anisotropic etching of (1 0 0) silicon, the electric and magnetic fields may not be always uniform and symmetrical. Further, when the electrode material is deposited on the side of the channel, it may result in non-parallel electrodes [7] which in turn could cause non-uniform electric fields. The 3D numerical framework developed in this study, therefore, provides a useful tool to model such non-uniformities.

(e) This work is also the first to report solution of the 3D MHD equations in the case of MHD pumps with trapezoidal cross-sections. Our work provides a more rational and thorough numerical framework for micropumps of arbitrary cross-sections than previous approximate results reported by Bao and Harrison [7] who investigated fluid velocities and flow rates for rectangular and trapezoidal sections using a simple Poiseuille type approximations.

(f) Numerical results reported here demonstrate that for an equivalent area of cross section and electrode length as well as current and magnetic flux densities, a trapezoidal cross-section MHD micropump could indeed give a comparable flow rate as that of rectangular cross-section MHD micropumps. Bao and Harrison [7] had used approximate formula applicable to macro channels under pressure-driven flows to report that trapezoidal cross-section MHD micropumps provided only one-third of the mean flow velocity and flow rate offered by rectangular cross-section micropumps. We think the major flaw in the approximate formula used arise from the inability of the model to take into account the effect of geometry on the variation of current and magnetic flux density at a cross-section. Only a model based on a full geometric descetization and solution of the most general MHD equations can predict these variations. It turns out that while there are significant local variations of the current and magnetic flux densities, the total integrated quantities at a given cross-section for both rectangular and trapezoidal cross-sections are comparable. The obvious implication of these results in flow rates is that trapezoidal cross-section MHD micropumps which are easier to micromachine through wet anisotropic etching of silicon than rectangular cross-section micropumps have a competitive advantage.

(g) The increased miniaturization of MHD micropumps to the range of tens of microns of characteristics dimensions that is being pursued by the research community [7,19] where the validity of continuum-based equations becomes questionable suggests that there still remains the need for extending the computational frameworks developed here and elsewhere to accommodate such miniaturizations.

Uncited references

[23,24,26–28].

References

[1] A.V. Lemoff, A.P. Lee, An ac magnetohydrodynamic micro-pump, Sens. Actuators B 63 (2000) 178–185.
[2] J. Jang, S.S. Lee, Theoretical and experimental study of MHD micropump, Sens. Actuators A 80 (2000) 84–89.
[3] L. Huang, W. Wang, M.C. Murphy, A lumped-parameter model for a micro-pump based on the magnetohydrodynamic (MHD) principle, Proc. SPIE–Design Test Microfabric. MEMS MOEMS 3680 (1999) 379–387.
[4] L. Huang, W. Wang, M.C. Murphy, K. Lian, Z.G. Ling, LIGA fabrication and test of a dc type magneto-hydrodynamic (MHD) micro-pump, Microsyst. Technol. 6 (2000) 235–240.
[5] K.H. Heng, L. Huang, W. Wang, M.C. Murphy, Development of a diffuser/nozzle type micro-pump based on magnetohydrodynamic (MHD) principle., Proc. SPIE—Microfluidic Devices Systems, II 3877 (1999) 66–73.
[6] K.H. Heng, W. Wang, M.C. Murphy, K. Lian, UV-LIGA microfabrication and test of an ac-type micro-pump based on the magnetohydrodynamic (MHD) principle, Proc. SPIE—Microfluidic Dev. Syst. III 4177 (2000) 174–184.
[7] J.B. Bao, D.J. Harrison, 2003. Design and Fabrication of Microchannels for Magnetohydrodynamic Flow, International Conference on MEMS, NANO and Smart Systems (ICMENS'03), Banff, Alberta, Canada, p. 396.
[8] P.J. Wang, C.Y. Chang, M.L. Chang, Biosens. Bioelectron. 20 (2004) 115–121.
[9] A. Homsy, S. Koster, J.C.T. Eijkel, A. Berg, F. Lucklum, E. Verpoorte, N.F. de Rooij, A high current density dc magnetohydrodynamic (MHD) micropump, Lab Chip 5 (4) (2005) 466–471.
[10] M. Hughes, K.A. Pericleous, M. Cross, The numerical modeling of dc electromagnetic pump and brake flow, Appl. Math. Model 19 (1995) 713–723.
[11] J.I. Ramos, N.S. Winowich, Finite difference and finite element methods for MHD flows, Int. J. Numer. Meth. Fluids 11 (1990) 907–934.
[12] N.S. Winowich, W.F. Hughes, J.I. Ramos, Numerical simulation of electromagnetic pump flow, Numer. Meth. Laminar Turbulent Flow 5 (2) (1987) 1228–1240.
[13] B. Singh, J. Lal, Finite element problems in magnetohydrodynamics and channel flow problems, Int. J. Numer. Meth. Eng. 15 (1982) 1104.
[14] R.F. Probstein, Physicochemical Hydrodynamics An Introduction, Wiley & Sons, New York, 1994.
[15] D. Erickson, D. Sinton, D. Li, Joule heating and heat transfer in poly(dimethylsiloxane) microfluidic systems, Lab Chip 3 (2003) 141–149.
[16] A. Ramos, H. Morgan, N.G. Green, A. Castellanos, ac electronics: a review of forces in microelectrode structures, J. Phys. D: Appl. Phys. 31 (1998) 2338–2353.

[17] M.S. Tillack, N.B. Morley, Magnetohydrodynamics Standard Handbook for Electrical Engineers, 14th ed., McGraw-Hill, 1998.
[18] FEMLAB FEA Software, Reference Manual, version 3.1, COMSOL, Inc., 2005.
[19] A.P. Lee, 2005. Personal communications.
[20] A. Olsson, P. Enoksson, G. Stemme, E. Stemme, Micromachined flat-walled valveless diffuser pumps, J. MEMS 6 (1997) 161–166.
[21] M. Heschel, M. Mullenborn, S. Bouwstr, Fabrication and characterization of truly 3D diffuser/nozzle microstructures in silicon, J. Microelectromech. Syst. (1997) 41–47.
[22] S. Bendib, O. Français, Analytical study of microchannel and passive microvalve application to micropump simulator, Proc. SPIE (1999) 200–208.
[23] M. Hughes, K.A. Pericleous, M. Cross, The CFD analysis of simple parabolic and elliptic MHD flows, Appl. Math. Model. 18 (1994) 150–155.
[24] O.C. Jeong, S.S. Yang, Fabrication and test of a thermo-pneumatic micro-pump with a corrugated p+ diaphragm, Sens. Actuators A 83 (2000) 249–255.
[25] N.J. Petersen, R.P.H. Nikolajsen, K.B. Mogensen, J.P. Kutter, Effect of Joule heating on efficiency and performance for microchip-based and capillary-based electrophoretic separation systems: a closer look, Electrophoresis 25 (2004) 253–269.
[26] E. Stemme, A. Stemme, A valveless diffuser nozzle-based fluid pump, Sens. Actuators A 39 (1993) 159–167.
[27] N.S. Winowich, W.F. Hughes, A finite element analysis of two-dimensional MHD flow, AIAA Prog. Astronaut. Aeronaut 84 (1983) 313.
[28] J. Zengerle, S. Ulrich, M. Kluge, A. Richter, Richter, A bidirectional silicon micropump, Sens. Actuators A 50 (1995) 81–86.